Wave–Turbulence Interactions in the Upper Ocean. Part II: Statistical Characteristics of Wave and Turbulent Components of the Random Velocity Field in the Marine Surface Layer

S. A. KITAIGORODSKII

Department of Earth and Planetary Sciences, The Johns Hopkins University, Baltimore, MD 21218

M. A. DONELAN

Canada Centre for Inland Waters, Burlington, Ontario, Canada L7R 4A6

J. L. LUMLEY AND E. A. TERRAY

Sibley School of Mechanical and Aerospace Engineering, Cornell University, Ithaca, NY 14850

(Manuscript received 24 January 1983, in final form 30 July 1983)

ABSTRACT

We present the results of an analysis of field data collected by Donelan who used a miniature drag sphere to measure velocities beneath wind waves on Lake Ontario. Linear statistical techniques are used to separate the velocity into wave and turbulent parts. While we mostly aim at demonstrating the effects of surface wind waves on the statistical characteristics of the turbulent field in the upper mixed layer, we also interpret several features of the data on the basis of recent theoretical results.

One of the most intriguing features of the turbulent velocity spectra so obtained is a large peak near the dominant wave frequency. We review various possible explanations for this behavior although we prefer a model in which the turbulence is assumed frozen on the timescale of the waves. This model requires no new dynamics and gives explicit formulae relating the dissipation rate to the magnitude of the spectral densities for high and low frequencies. On this basis we have determined a dissipation length from the data. The dependence of this quantity on depth is inconsistent with pure shear produced turbulence. Moreover the observed rms turbulent velocities show a strong dependence on wave energy, which cannot be explained solely within the framework of similarity theory for the inner (constant flux) layer.

1. Introduction

In the first paper of this series (Kitaigorodskii and Lumley, 1983, hereafter referred to as P1) we proposed that the statistical dynamics of turbulence, in the presence of surface waves, can be described by assuming that the potential and rotational components of the net velocity field are uncorrelated. This hypothesis (an attempt was made in P1 to justify it theoretically) is also widely used to process and interpret data in the surface layer of the sea when simultaneous measurements of velocity fluctuations and sea surface displacements are available (Kitaigorodskii, 1973). In this case the functional relationship between the wave-induced part of the velocity field and the surface displacement due to wind waves can be considered to be deterministic, which in turn permits the use of linear filtration techniques as an acceptable approximation for the separation of wave and turbulent motions (Benilov and Filushkin, 1970). We use this procedure to analyze the field data collected by Donelan (1978) using a miniature drag sphere velocimeter. While we mostly aim at demonstrating the effects of surface wind waves on the statistical characteristics of the turbulent field in the upper surface layer of the sea, we will also attempt to interpret several features of oceanic turbulence in the presence of random wind waves on the basis of the theoretical results reported in P1.

2. Method of linear filtration in the analysis of fluctuations of random fields in the upper ocean in the presence of wind waves

Following the discussion in P1 we define the turbulent and wave velocities as, respectively, the rotational and potential parts of the fluctuating velocity. Similarly we write the net pressure as

$$p = P(z) + p_t + p_\phi, \tag{1}$$

where $P(z)$ is the mean pressure and $p_t + p_\phi$ is the fluctuating component. We define p_ϕ via the linearized Bernoulli equation

$$\nabla\left[\partial_t\phi + gz + \frac{1}{\rho}(P(z) + p_\phi)\right] = 0, \tag{2}$$

where ϕ is the velocity potential, $\mathbf{u}^w = \nabla\phi$. Using (2), the Navier–Stokes equation reduces to

$$(\partial_t - \nu\nabla^2)\mathbf{u}^t + (\mathbf{u}^t\cdot\nabla)\mathbf{u}^t - \langle(\mathbf{u}^t\cdot\nabla)\mathbf{u}^t\rangle + (\mathbf{u}^t\cdot\nabla)\mathbf{U} + (\mathbf{U}\cdot\nabla)\mathbf{u}^t + \mathbf{Q} = -\nabla\left[\frac{p_t}{\rho} + \frac{1}{2}(u^w)^2 - \frac{1}{2}\langle(u^w)^2\rangle\right], \quad (3)$$

where $\mathbf{U}$ is the mean velocity, and

$$\mathbf{Q} = (\mathbf{u}^t\cdot\nabla)\mathbf{u}^w - \langle(\mathbf{u}^t\cdot\nabla)\mathbf{u}^w\rangle + (\mathbf{u}^w\cdot\nabla)\mathbf{u}^t - \langle(\mathbf{u}^w\cdot\nabla)\mathbf{u}^t\rangle + (\mathbf{U}\cdot\nabla)\mathbf{u}^w + (\mathbf{u}^w\cdot\nabla)\mathbf{U}. \quad (4)$$

Note contributions to p_t will include the effects of nonlinearity in the wave motion and therefore the turbulent field $\mathbf{u}^t$ in Eq. (3) must, in principle, be corrected by excluding the *forced nonlinear potential wave components.* However the role of the latter in the energy balance of the fluctuating motions in the upper ocean is probably not very important (see P1), so that Eq. (3), with a given random velocity field $\mathbf{u}^w$, can be considered to govern the turbulent velocity and pressure fluctuations. The potential motions satisfy Laplace's equation with the *linearized* kinematic boundary condition

$$u_3^w - \frac{d\zeta}{dt} = u_j^t\partial_j\zeta \quad \text{at} \quad z = 0, \quad (5)$$

where $j = 1, 2$, $d/dt = \partial_t + \mathbf{U}\cdot\nabla$, and ζ is the surface displacement. The other boundary condition, appropriate to the deep ocean, takes form

$$u_3^w \to 0 \quad \text{for} \quad z \to \infty. \quad (6)$$

Because typically $u^t/u^w \ll 1$ the boundary conditions on ϕ are approximately independent of the turbulence (at least for turbulence with scales comparable to the scale of the waves). Consequently the wave velocity can, for our purposes, be considered as a deterministic functional of the surface displacement. For simplicity we further presume the relation to be linear. Then

$$\mathbf{u}^w(\mathbf{x}, z, t) = \mathbf{L}[\zeta]. \quad (7)$$

Here $\mathbf{x} = (x_1, x_2)$ is in the horizontal plane, and L is a vectorial, linear, space-time operator depending on the vertical coordinate z. Denoting its spectral characteristic by $\mathbf{G}(\kappa, w, z)$, we have

$$\mathbf{u}^w(\mathbf{x}, z, t) = \int \mathbf{G}(\kappa, \omega, z)e^{i(\kappa\cdot\mathbf{x}-\omega t)}dZ_\zeta(\kappa, \omega), \quad (8)$$

where $dZ_\zeta(\kappa, \omega)$ is the Fourier–Stieltjes coefficient of ζ and the integration is performed over the whole domain (κ, ω). If the wave and turbulent fluctuations are uncorrelated, i.e.,

$$\langle u_i^t(\mathbf{x}, z, t)u_j^w(\mathbf{x}', z', t')\rangle = 0. \quad (9)$$

Then an unbiased estimate of the spectral components, $G_i(\kappa, \omega, z)$, of the operator L in (8) is given by the formulae

$$G_i(\kappa, \omega, z) = \Psi_{i\zeta}(\kappa, \omega, z)/\Psi_\zeta(\kappa, \omega), \quad (10)$$

where $\Psi_{i\zeta}(\kappa, \omega, z)(i = 1, 2, 3)$ is the "cross-spectrum" of the fluctuating velocity, $\mathbf{u}^t = \mathbf{u}^t + \mathbf{u}^w$, and the wave height, ζ and $\psi_\zeta(\kappa, \omega)$ is the wavenumber frequency spectrum of ζ. Therefore equations (8)–(10) completely determine the wave and turbulent components of the random velocity field in the upper surface layer. However, in practical applications of this technique the fields $\mathbf{u}^t$ and ζ are usually known as random functions of time at some fixed point in space. In such a case one can speak only of estimates $[\mathbf{u}^t]_E$ and $[\mathbf{u}^w]_E$ when separating the realizations of the fluctuating velocity field into turbulent and wave components.

The optimal estimate of the wave component $\mathbf{u}^w$

$$[u_i^w]_E = H[\zeta] \quad (11)$$

takes the form

$$[u_i^w]_E = \int e^{-i\omega t}P_i(\omega, z)dZ_\zeta'(\mathbf{x}, \omega), \quad (12)$$

where

$$P_i(\omega, z) = \frac{F_{i\zeta}(\omega, z)}{F_\zeta(\omega)} \quad (13)$$

and

$$F_{i\zeta}(\omega, z) = \int \Psi_{i\zeta}(\kappa, \omega, z)d\kappa,$$
$$F_\zeta(\omega) = \int \Psi_\zeta(\kappa, \omega)d\kappa. \quad (14)$$

We denote the magnitude of the rms error of the estimate (12), which is also the error of filtration, by the formula

$$\sigma_i^2 = \langle(u_i^w - [u_i^w]_E)^2\rangle. \quad (15)$$

Then (Benilov and Filushkin, 1970, Benilov, 1978)

$$\sigma_i^2 = \int d\omega\left[\int d\kappa|G_i(\kappa, \omega, z)|^2\Psi_\zeta(\kappa, \omega) - |P_i(\omega, z)|^2F_\zeta(\omega)\right]. \quad (16)$$

According to the linear theory of small amplitude surface gravity waves the spectral characteristic, $G_3(\kappa, \omega, z)$, of the operator L in (8) is independent of the direction of the vector κ. Consequently the spectral characteristic $P_3(\omega, z)$ equals $G_3[\kappa(\omega), \omega, z]$, where $\kappa(\omega) = \omega^2/g$ for deep water, and thus

$$\sigma_3^2 = 0. \quad (17)$$

But for the horizontal velocity components, according to linear wave theory,

$$G_i(\kappa, \omega, z) = \frac{\kappa_i\omega}{|\kappa|}e^{-|\kappa|z}, \quad i = 1, 2; \quad z \geqslant 0, \quad (18)$$

and therefore σ_1 and σ_2 differ from zero and depend on the angular energy distribution in the wave spectrum

$\psi_{\zeta\zeta}(\kappa, \omega)$. Because of this the low coherence level $\gamma^2_{i\zeta} \equiv (F_{i\zeta})^2/F_{\zeta\zeta}F_{ii}$ between ζ and the measured fluctuating velocity field u'_i does not necessarily imply the absence of a wave-like contribution; it can be related to the angular distribution in the spatial wave spectrum and to the direction of wave propagation relative to the coordinate system associated with the velocimeter. It was shown (Benilov, 1978) that the relative error of filtration $\sigma^2_i/(u^w_1)^2$ is minimized when the general direction of wave propagation coincides with the x_1 axis of the coordinate system associated with the velocimeter. Consequently the most reliable estimates of u^w_i and hence u'_i, using the linear filtration technique, will be for the vertical velocity components. With this in mind we present in the next sections the results of the determination of the statistical characteristics of the wave and turbulent components of the velocity field on the basis of *in situ* field measurements of velocity fluctuations beneath wind-generated waves.

3. General description of measurements

Measurements of velocity components beneath natural, wind-generated waves have been obtained from a fixed tower on Lake Ontario. The field site, described fully by Birch *et al.* (1976), is a bottom-mounted tower installed in 12.5 meters of water and 1.1 km from the western end of the lake. Designed specifically for wave research, the tower is free of cross bracing from 4 m above still water level to 6 m below. In this region the only disturbances to the flow are the four cylindrical legs of 40 cm diameter on the corners of a 10.7 m $\times$ 10.7 m square at the surface, and angled towards the center at 10 deg to the vertical. The velocity components were sensed by a drag sphere velocimeter, specially developed for the measurement of three dimensional turbulence embedded in a highly oscillatory flow, (Donelan and Motycka, 1978, Donelan 1978). It was mounted on a vertical track mid-way between the two offshore legs. The vertical track is of ellipsoidal section (30 cm $\times$ 19 cm) and was rotated so that its major axis was aligned with the expected wave direction during data-gathering. The drag sphere was attached to the track on a horizontal arm 90 cm long and could be positioned at depths to 6 m. Two capacitance wave staffs were attached to the track at 61 cm on either side of the center of the track along its minor axis. The wave staff nearer the drag sphere provided surface elevation information simultaneous with the velocity data. The pair of wave staffs, since they were rotated with the track and drag sphere, yielded some rudimentary information on the approach direction of the waves. Temperature fluctuations were sensed by a small thermistor mounted on the velocimeter support arm. The position changes of the arm and data collection operations were controlled from the recording station on shore, where the returning digital data were stored on magnetic tape for later processing. Wind speed and direction were measured at a height of 11.6 m. The velocimeter and thermistor signals were sampled 20 times per second, while the other channels were sampled 5 times per second. Among 14 runs which have been analyzed, 4 were isolated and chosen for analysis. These were the only ones which satisfied the following criteria: 1) single peaked wave (surface displacement) spectrum $E_{\zeta\zeta}(\omega)$; and 2) the peak wave direction and the orientation of the drag sphere did not differ by more than 30°. During those runs velocity measurements were made in the region below the wave troughs down to 5 m (the closest level to the surface was 29 cm). Simultaneous measurements of surface wind waves covered a range of variation in significant wave height $H_{1/3}$ from 0.26 to 0.58 m, whereas mean wind varied from 6 to 11 m s^{-1}. As a rule the situations examined correspond to active wind–wave generation conditions for short fetches. The wind stress τ_0 was estimated using the experimental value of the drag coefficient $C_{10} \approx 1.5 \times 10^{-3}$ appropriate for these conditions (Donelan, 1982) so that the characteristic velocity scale u_* for turbulent motions in water can be calculated as

$$u_* = U_{10}\left[C_{10}\frac{\rho_a}{\rho_w}\right]^{1/2}, \tag{19}$$

where U_{10} is the wind speed measured on the tower.

Direct measurements of the Reynolds stresses by the drag sphere have confirmed the approximate agreement between the momentum flux in the water, $\tau = \rho_w\langle u_1 u_3\rangle = \rho_w u_*^2$ to wind stress, $\tau_a = \rho_a C_{10} U_{10}^2$ (Donelan, 1978).

In order to use the linear filtration technique, described in Section 2, the spectral densities $F_{1\zeta}(\omega)$, $F_{3\zeta}(\omega)$ and $F_{\zeta\zeta}(\omega)$ were computed by partitioning the data into several pieces, fast fourier transforming each segment and then averaging the resulting spectral estimates to obtain the spectra of the separated velocity components $\mathbf{u}^w$ and $\mathbf{u}'$. The spectral estimates are indicated by crosses in which the vertical bar is twice the standard error of the estimates among the separately transformed segments within a run. The averaged characteristics of the runs selected are presented in Table 1. We have retained only those data satisfying the requirement that the external conditions changed by less than 15% during the course of the run. Table 2 summarizes the depth dependence of various rms quantities.

4. The statistical characteristics of the wave induced velocity field

Typical frequency spectra for vertical u^w_3 and horizontal u^w_1 wave velocities are shown in Figs. 1b and c. The corresponding wave height spectrum is shown in Fig. 1a. All the spectra in Fig. 1 are normalized to unit area and are plotted as functions of f/f_p, where f_p corresponds to the peak of the wave-height spectrum.

TABLE 1. Average characteristics of the data.

Run	Number depths sampled	Max/Min depth (m)	Duration of run (min)	U_{10} (m s^{-1})	u_* (cm s^{-1})	ζ_{rms} (cm)	ω_p (s^{-1})	k_p (m^{-1})	$\tau_p = \frac{2\pi}{\omega_p}$ (s)	$\lambda_p = \frac{2\pi}{\kappa_p}$ (m)	$C_p = \frac{\omega_p}{\kappa_p}$ (m/s)	$\frac{U_{10}}{C_p}$	$k_p\zeta_{rms}$
1	4	0.52/1.70	65	6.1	0.83	8.1	2.62	0.70	2.4	9.0	3.75	1.61	0.056
2	5	0.82/4.88	27	5.8	0.80	14.5	1.93	0.38	3.3	16.6	5.09	1.00	0.055
3	4	0.29/0.89	56	10.7	1.47	6.6	3.55	1.28	1.8	4.9	2.77	3.86	0.085
4	5	0.41/1.17	81	11.2	1.54	6.4	3.61	1.33	1.7	4.7	2.72	4.11	0.085

The peak frequency is the same in these three spectra, and the much more rapid decrease of velocity fluctuations compared with the wave height for frequencies greater than the peak is pronounced. The simplest way to verify the predictions of linear wave theory for such spectra is to estimate the wave-induced rms velocities $\langle(u_1^w)^2\rangle^{1/2} = \sigma_1^w$ and $\langle(u_3^w)^2\rangle^{1/2} = \sigma_3^w$. If most of the wave energy propagates in the peak wave direction (along x_1) then according to linear theory we can estimate σ_1^w as

$$\sigma_1^{w2} \approx \int_0^\infty d\omega\omega^2 e^{-2\omega^2 z/g} F_\zeta(\omega). \tag{20}$$

Introducing the concept of an "equivalent dominant wave" with frequency ω_p, i.e. assuming

$$F_\zeta(\omega) = \zeta_{rms}^2 \delta(\omega - \omega_P), \tag{21}$$

where

$$\zeta_{rms}^2 = \int_0^\infty d\omega F_\zeta(\omega), \tag{22}$$

we can estimate σ_1^w as

$$\sigma_1^w = \sigma_P e^{-k_P z}, \tag{23}$$

where $k_p = \omega_p^2/g$ and $\sigma_p = \omega_p\zeta_{rms}$.

We have fit the observed ratio σ_1^w/σ_p with the simple exponential depth dependence

$$\frac{\sigma_{1,3}^w}{\sigma_P} = A_{1,3}^w e^{-a_{1,3}^w \kappa_P z}. \tag{24}$$

Both horizontal and vertical rms wave velocities, scaled by σ_p, are displayed in Fig. 2. Plots showing the greatest amount of scatter are associated with the greatest variation of the velocity scale σ_p.

There also appears to be some systematic departure from a simple exponential form at the extremes in z.

Table 3 summarizes the least square fit to the parameters $A_{1,3}^w$ and $a_{1,3}^w$ appearing in Eq. (24). These coefficients are approximately equal to unity which indicates that the rms wave velocities are reasonably accounted for by an "equivalent dominant wave", although such a simplified parameterization consistently gives a slight overestimate to the data. Because our primary goal here is not to compare the statistical characteristics of $\mathbf{u}^w$ with the predictions of linear wave theory, we did not try to fit the observed wave-induced velocity spectra, $F_{ii}(\omega)$, using the data on the wave spectra $F_\zeta(\omega)$ [one example of this was presented by Donelan (1978)]. Instead we prefer to place more at-

TABLE 2. Detailed characteristics of the data.

Run	z (m)	Length of record (sec)	k_pz	ω_p (s^{-1})	ζ_{rms} (cm)	U_D (cm s^{-1})	σ_1^w (cm s^{-1})	σ_3^w (cm s^{-1})	u_*	σ_1' (cm s^{-1})	σ_3' (cm s^{-1})
	0.52	985	0.36	2.62	7.66	7.74	12.20	14.44	0.85	5.92	5.39
1	0.92	966	0.65	2.64	7.68	8.19	8.82	10.62	0.77	4.54	3.81
	1.32	966	0.92	2.62	8.08	8.25	6.73	8.53	0.88	3.98	3.21
	1.70	966	1.16	2.59	8.87	6.03	6.55	7.83	0.86	3.91	3.07
	0.82	338	0.31	1.93	15.72	−2.92	20.02	20.00	0.71	7.68	10.06
	1.82	310	0.68	1.91	14.66	−5.80	13.10	14.50	0.76	4.30	3.71
2	2.83	291	1.06	1.92	14.66	−6.33	8.20	9.03	0.81	3.70	3.32
	3.84	323	1.49	1.95	14.25	−3.79	4.96	5.91	0.85	3.38	3.43
	4.88	347	1.85	1.93	13.30	−4.85	3.38	3.95	0.90	2.51	3.67
	0.29	944	0.38	3.58	6.50	−8.76	14.97	16.41	1.48	8.73	8.75
3	0.44	734	0.56	3.53	6.85	−10.98	12.79	14.19	1.49	7.01	6.56
	0.62	910	0.77	3.50	6.60	−10.52	9.40	10.21	1.58	6.01	5.29
	0.89	771	1.16	3.57	6.47	−12.49	5.68	6.65	1.38	4.33	3.88
	0.41	970	0.54	3.58	6.36	−4.00	13.81	13.32	1.58	7.29	6.65
	0.63	966	0.89	3.73	6.32	−4.44	10.00	9.83	1.52	5.47	5.46
4	0.67	1026	0.92	3.67	6.16	−9.03	7.68	8.52	1.45	5.84	4.77
	0.87	949	1.14	3.58	6.40	−4.92	6.99	7.40	1.57	5.17	4.44
	1.17	966	1.47	3.51	6.60	−8.01	5.53	5.63	1.65	4.80	3.71

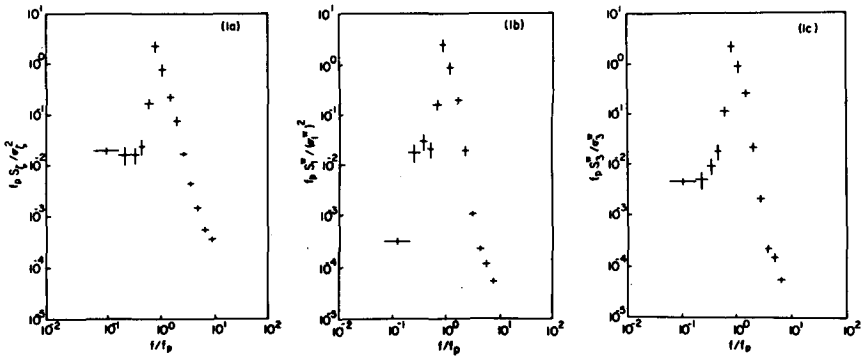

FIG. 1. Wave height, longitudinal and vertical wave velocity spectra taken from Run 2, $z = 0.82$ m, normalized to unit area versus frequency. The f_p is the peak wave frequency.

tention on the variability of the turbulent velocity field $\mathbf{u}'$.

5. The spectra of the turbulent velocity field u in the presence of wind waves

Typical spectra of the turbulent velocities are given in Figs. 3a, b. These spectra correspond to the wave spectra shown in Fig. 1a and are similarly normalized to unit area. The most prominent feature of the turbulent spectra is the pronounced enhancement about the peak wave frequency, f_p. Analysis of the turbulent spectra at different depths has shown that this "bump" appears to be roughly independent of depth, but is rather sensitive to wave conditions. The other very interesting feature of the turbulent spectra is that both above and below f_p the frequency dependence tends to be close to $f^{-5/3}$, but there is a consistent shift to larger values of spectral density for frequencies above the peak. These two features probably are interrelated and their explanation presents a very intriguing problem in the dynamics of upper layer turbulence in the presence of wind waves. Several explanations can be suggested and must be analyzed. We list some of them as follows:

1) The errors in linear filtration are greatest at frequencies $f \approx f_p$, and therefore the enhancement about f_p may be due to such errors. However such enhancements are also strongly pronounced in the spectra of *vertical* turbulent components, in which the errors of linear filtration associated with the directionality of the wave spectrum are identically zero. The other possible source of errors in the separation of the velocity field into turbulent and wave components can be attributed to the nonlinearity in the dependence of the wave velocity on the wave height, which is not taken into account by the linear filtration procedure. Corrections of this type can be estimated, and such estimates show that their contribution is small. It is also difficult to see how they would contribute to the in-

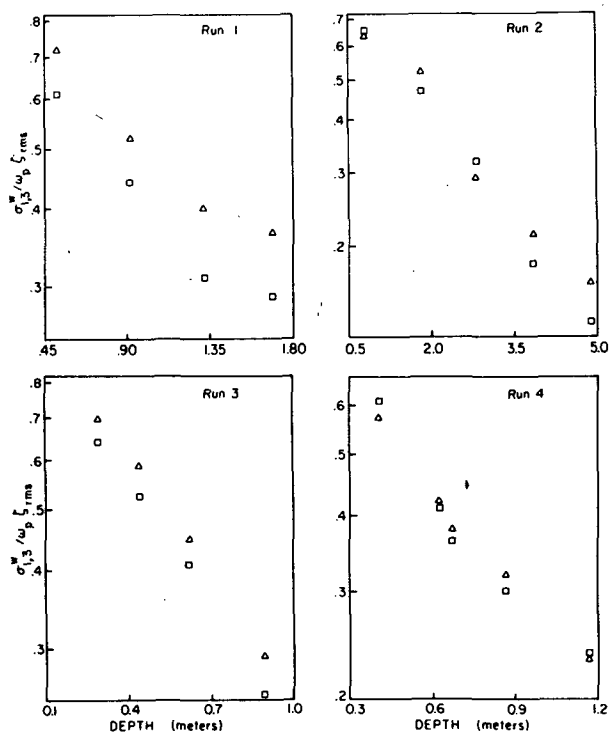

FIG. 2. Normalized vertical (triangles) and longitudinal (squares) rms wave velocities versus depth for all runs.

TABLE 3. Fit parameters to the normalized longitudinal (1) and vertical (3) rms wave velocities.

$$\frac{\sigma^w_{1,3}}{\zeta_{rms}\omega_p} = A^w_{1,3}\exp(-a^w_{1,3}k_p z)$$

Run	k_p (m^{-1})	A^w_1	a^w_1	A^w_3	a^w_3
1	0.70	0.82	0.94	0.97	0.91
2	0.38	0.95	1.11	0.93	0.97
3	1.28	1.04	1.23	1.11	1.16
4	1.33	0.88	0.89	0.87	0.85

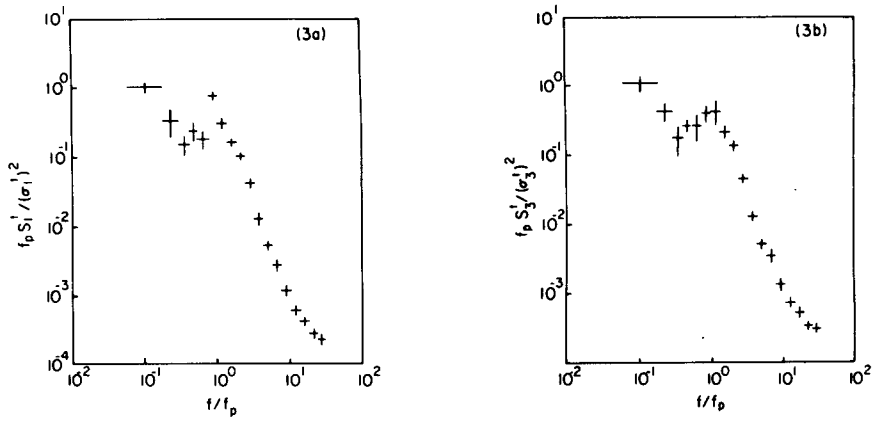

FIG. 3. As in Fig. 1 but for longitudinal and vertical turbulent velocity spectra.

creased spectral densities for frequencies greater than f_p.

2) A cause of the peak in the spectra of the turbulent velocity components near the wave frequency, even though there is no coherence with the surface displacement ζ, may be related to the coupling of the lateral separation (40 cm or so) of the wave staff and velocimeter with the observed short-crestedness (lateral variation) of the waves. However the peak appears to be just as pronounced for the 16 meter long gentle waves of run 2 as it is for the 5 meter steep waves of runs 3 and 4 suggesting that this is not a problem.

3) One convenient explanation of the two main specific features of the turbulent spectra can be made by assuming that near the peak wave frequency there is a region of additional energy supply to the turbulence. Presumably this is due to the transformation of wave energy to turbulence as a result of wave turbulence interactions (or even wave breaking). Actually it was hypothesized long ago by Ozmidov (1968) that the spectra of oceanic turbulence would show different inertial subranges separated by narrow zones (bumps), where some specific mechanism of direct energy supply interrupts (or adds energy to) the turbulent cascade process which is transporting energy from large to small scales. One such zone can presumably be associated with surface waves, and therefore the higher level of energy in the $f^{-5/3}$ region below the peak frequency ($f < f_p$) compared with the $f^{-5/3}$ region above it ($f > f_p$), is a consequence of different energy fluxes through the wavenumber space. This energy flux can be simultaneously considered as a *mean viscous dissipation* in the region above the peak only if there is no additional energy supply between the wave scales and the Kolmogorov microscale of the turbulence. The attractiveness of such a hypothesis is evident; however, not much can be said for its support. If one of the main mechanisms of the transformation of surface wave energy into turbulence energy is wave breaking, it does not necessarily mean that the source of turbulent energy associated with breaking must be near the wave peak. A more serious objection to wave breaking as a reason for the observed bumps in turbulent spectra comes from the observation, mentioned above, that such bumps are roughly depth-independent and exist at levels relatively far from the mean water level, where the direct effect of breaking on turbulence is probably very small. More to the point, as was discussed in P1, the shear produced three-dimensional turbulence in the surface layer of the sea must appear at frequencies below the wave peak, and the interactions between waves and shear turbulence can be pronounced only in the range of frequencies lower (or much lower) than the peak wave frequency. Therefore we do not completely disregard the idea that the waves can supply energy directly to the turbulence at frequencies $f \sim f_p$, but at present we cannot find direct proof of such a hypothesis.

Although we cannot categorically disprove any of the mechanisms listed above we believe there exists a simpler and more direct explanation, which we review in the next section, for the structure of the observed turbulent spectra.

6. The influence of surface waves on the shape of the turbulence spectra

This model has been discussed elsewhere (Lumley and Terray, 1983) and so our discussion here will be brief. The mechanism envisioned is a generalization of the usual Taylor frozen turbulence hypothesis to the case where the convecting velocity has periodic components. It is important to note that the model does not introduce any new dynamics—the background turbulence is presumed to be homogeneous and isotropic with an inertial range spectral density $E(\kappa)$ given by

$$E(\kappa) = c\epsilon^{2/3}\kappa^{-5/3}. \tag{25}$$

Roughly speaking a typical turbulent fluctuation with characteristic size κ^{-1} will appear frozen if its dynamical time scale, $\tau_t \approx \epsilon^{-1/3}\kappa^{-2/3}$, is long compared

with the time, $\tau_c \approx (kU_c)^{-1}$, required to convect it past the probe. Here U_c is the convecting velocity (orbital or drift), and ϵ is the rate of energy transfer to the turbulence. Then the condition $\tau_t \gg \tau_c$ can be written

$$\kappa l \gg \left(\frac{u}{U_c}\right)^3, \tag{26}$$

where u is the rms turbulent velocity and we use the estimate $\epsilon \approx u^3/l$. Since for our data the rhs is typically much smaller than 1 we expect the whole of the inertial subrange will be frozen. If the convecting velocity is periodic in time with frequency f_p it is immediately clear that the frequency spectrum will consist of lines at multiples of f_p. Two mechanisms for broadening these lines are apparent: the first is to suppose that the orbital velocities are themselves random functions of time while the second is to superimpose a constant longitudinal drift with velocity U_D. In the latter case, the degree of broadening each line experiences will depend on the ratio of orbital to drift velocities, $\omega_p \zeta_{\text{rms}}/U_D$. For large values of this ratio the spectrum will show considerable structure about $n\omega_p$, ($\omega_p = 2\pi f_p$), tending ultimately to the line spectrum found earlier. We can also distinguish two frequency regimes. For $\omega \to 0$ we expect that we can neglect the orbital velocity with respect to the drift. Then we recover the well-known case of uniform translation, and the spectra $S_{1,3}(\omega)$ are given by

$$S_{1,3}(\omega) = \frac{2}{U_D} F_{1,3}\left(\frac{\omega}{U_D}\right), \tag{27}$$

where $F_{1,3}$ are the one-dimensional longitudinal and transverse spectra (normalized to $\langle u_1'^2 \rangle$ and $\langle u_3'^2 \rangle$ respectively). In the inertial subrange

$$S_1 = \frac{18}{55} C\epsilon^{2/3} U_D^{2/3} \omega^{-5/3}, \quad \omega \ll \omega_p, \tag{28}$$

and $S_3 = \frac{4}{3} S_1$.

In the other limit, $\omega \to \infty$, the orbital motions dominate, and the situation is more complex. Such motions "sample" the turbulence periodically in two directions, and so modulate between the longitudinal and transverse spectra, producing an average.

Asymptotically the spectra are proportional to

$$S_{1,3} \approx C\epsilon^{2/3} \sigma_w^{2/3} \omega^{-5/3}, \quad \omega_p \ll \omega, \tag{29}$$

where σ_w is the rms wave orbital velocity, and the constant of proportionality depends on details of the wave spectrum. Combining the estimates in Eq. (28) and (29) we find

$$\frac{S(\omega \gg \omega_p)}{S(\omega \ll \omega_p)} \approx \left(\frac{\sigma_w}{U_D}\right)^{2/3} > 1. \tag{30}$$

Consequently the model outlined above shows that the shape of the observed turbulent spectra (strong enhancements at f_p and increased spectral densities for $f \gg f_p$) does not necessarily imply a direct wave–turbulence interaction in the range of observed frequencies. It also allows estimates of the *dissipation rate* ϵ to be made from the observed spectra and measured values of the drift current.

The effects described here also apply to passively convected scalars. Consequently, the spectra of temperature fluctuations provide an independent test of the model. In Fig. 4 we show the turbulent temperature spectrum from run 1 $z = 0.52$ m, obtained via linear filtration, along with the corresponding spectrum of the longitudinal turbulent velocity, u_1'. For this case the temperature gradient (0.03°C m^{-1}) is very small so that the temperature can be regarded as an essentially passive scalar. In addition the mean temperature (4.7°C) is near the point of maximum density. As in the turbulent velocity spectra there is evidence of a peak at the wave frequency, although it is much less pronounced. However, this is to be expected since temperature fluctuations are simply being advected

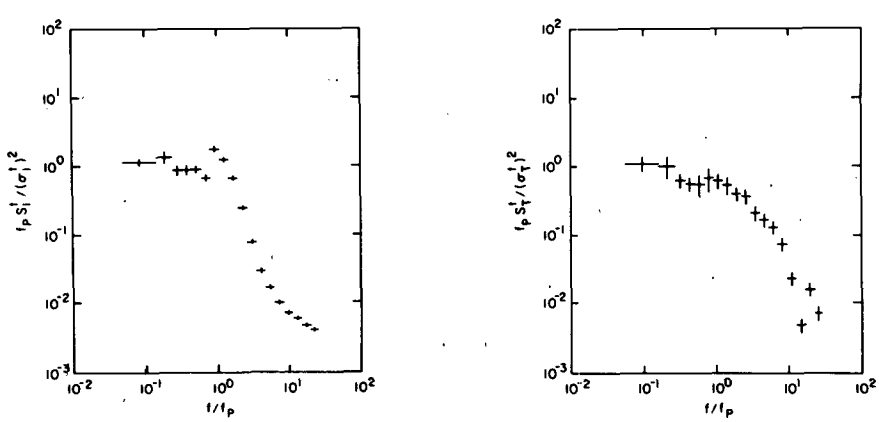

FIG. 4. Longitudinal turbulent velocity and turbulent temperature spectra taken from Run 1, $z = 0.52$ m, normalized to unit area versus frequency. $\sigma_T' = 2.9$ m °C is the rms turbulent temperature and f_p is the peak wave frequency.

past the probe by the wave orbital motion; whereas in the case of the velocity field there is an additional orientational modulation between longitudinal and vertical velocity components.

Since ϵ appears as a free parameter, this model sidesteps the more fundamental question of the dynamical influence of the wave motions on the turbulence. Consequently we consider in the next section the dependence of both the rms turbulent velocities and the energy dissipation rate ϵ on wave conditions.

7. The variability of rms turbulent velocities and energy dissipation in the surface layer of the sea beneath wind waves

As was mentioned in Section 3, one of the natural characteristic velocity scales for turbulent motions in water u_* can be estimated from the wind speed since the drag coefficient is known. In general this estimate of u_* is reasonably well correlated with the measured values of the Reynolds stress $\langle u_1' u_3' \rangle^{1/2}$ although it consistently underestimates the magnitude. However, u_* varies relatively slowly and so we will use it to normalize the rms turbulent velocities.

The measured values of both horizontal and vertical rms turbulent velocities, $\sigma_{1,3}^t = \langle u_{1,3}^{t2} \rangle^{1/2}$, appear in Fig. 5. These data show that the turbulent intensities fall off roughly exponentially with depth in the first 1.5 meters, while below this the rate of decrease is substantially smaller. A reasonable fit to the behavior of $\sigma_{1,3}^t$ for $Z \leqslant 1.5$ meters is given by

$$\frac{\sigma_{1,3}^t}{u_*} = A_{1,3}^t e^{-a_{1,3}^t k_p z}, \tag{31}$$

where k_p is the peak wavenumber, $k_p = \omega_p^2/g$.

The result of a least square fit for the values of the parameters $a_{1,3}^t$ and $A_{1,3}^t$ is summarized in Table 4. The values of $a_{1,3}^t$ fluctuate about a mean of $\approx \frac{2}{3}$ and are consistently smaller than their counterparts for the wave motion, $a_{1,3}^w \approx 1$. We have further investigated the dependence of $A_{1,3}^t$ on various dimensionless ratios characterizing the sea state. According to the simple model of the energy balance of turbulence beneath waves, proposed in P1, we can expect a variation of $A_{1,3}^t$ with the nondimensional ratio $\omega_p \zeta_{\text{rms}}/u_*$, where ζ_{rms}, ω_p and u_* here represent averages over a given run (see Table 1). The relationship is shown in Fig. 6. There is no significant difference in the behavior of A_1^t and A_3^t within the ranges shown. Taking all of the points together, a least-square fit is given by:

$$A_{1,3}^t = 0.3\left(\frac{\omega_p \zeta_{\text{rms}}}{u_*}\right) + 2.7; \quad 15 \leqslant \frac{\omega_p \zeta_{\text{rms}}}{u_*} \leqslant 25. \tag{32}$$

According to the theory proposed in P1

$$\sigma_{1,3}^t = u_* A_{1,3}(k_p z, \sigma_w/u_*). \tag{33}$$

In the empirical relationship (31) $a_{1,3}^t \approx 1$ and thus

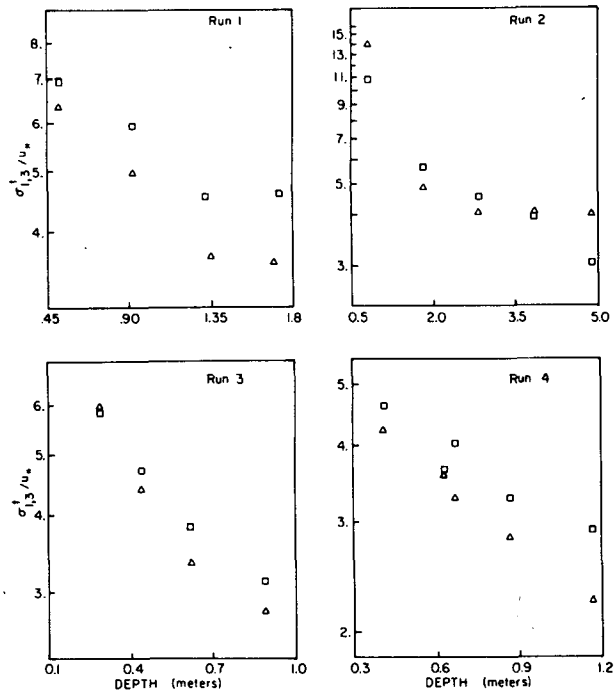

FIG. 5. As in Fig. 2 but for turbulent velocities.

for $k_p z \to 0$ ($k_p \to 0$ because $z \gg z_0$) formulae (33) yields (see P1)

$$\sigma_{1,3}^t \to u_* A_{1,3}^t\left(\frac{\sigma_w}{u_*}\right). \tag{34}$$

The asymptotic behavior of the function A_{10}, predicted in P1, is

$$A_{1,3}^t \to \alpha_{1,3} \quad \text{for} \quad \frac{\sigma_w}{u_*} \to 0, \tag{35}$$

$$A_{1,3}^t \to \frac{\beta_{1,3}\sigma_w}{u_*} \quad \text{for} \quad \frac{\sigma_w}{u_*} \to \infty, \tag{36}$$

where $\alpha_{1,3}$ and $\beta_{1,3}$ are numbers, and can be considered known from the well documented relationships in the constant flux surface shear layer. The collection of such data shows that $\alpha_1 \approx 2.3$ and $\alpha_3 \approx 0.9$ (Monin and Yaglom, 1971 Part 1). Although we do not observe any difference between A_1^t and A_3^t in the range studied, our data is not inconsistent with the asymptotic values $\alpha_{1,3}$ appropriate to the shear layer.

To find an estimate for the dissipation we have isolated (in the spirit of the model presented in the last section) seven spectra which show a well-developed "inertial range". Since the Reynolds numbers for these cases are only a few thousand it is not too surprising that we have only been able to find a small number of spectra exhibiting an $f^{-5/3}$ behavior for $f < f_p$. Using the measured value of the drift velocity U_D and the low frequency form of the spectrum given by equation (28) (we use $C \approx 1.5$), we can determine ϵ and subsequently l via the definition $\epsilon \equiv q^3/l$, where q^2

TABLE 4. Fit parameters to the normalized longitudinal (1) and vertical (3) rms turbulent velocities.

$$\frac{\sigma'_{1,3}}{u_*} = A'_{1,3}\exp(-a'_{1,3}k_p z)$$

Run	$\frac{\omega_p \zeta_{rms}}{u_*}$	A'_1	a'_1	A'_3	a'_3
1	25.6	9.4	0.82	9.2	1.08
3	15.9	7.6	0.66	7.9	0.82
4	15.0	5.7	0.50	5.9	0.73

$= \frac{1}{2}\langle \sigma_1'^2 + \sigma_3'^2 \rangle$. Fig. 7 shows six normalized low frequency spectra for the horizontal turbulent velocity, $U_D S_1/lq^2$, plotted against lf/U_D. The reference line shown has slope $-5/3$.

The values of ϵ and l within the topmost meter are given in Table 5. We find a dissipation rate of order 1 cm^2 s^{-3} which is two orders of magnitude larger than the expected value for a constant stress layer. For the latter case we can estimate

$$\epsilon_{\substack{\text{constant}\\ \text{stress}}} = \frac{u_*^3}{\kappa z} \approx 10^{-2}\ \text{cm}^2\ \text{s}^{-3}, \qquad (37)$$

where $\kappa = 0.4$ is the von Karman constant. Although such large dissipation is, at first sight, unsettling, the

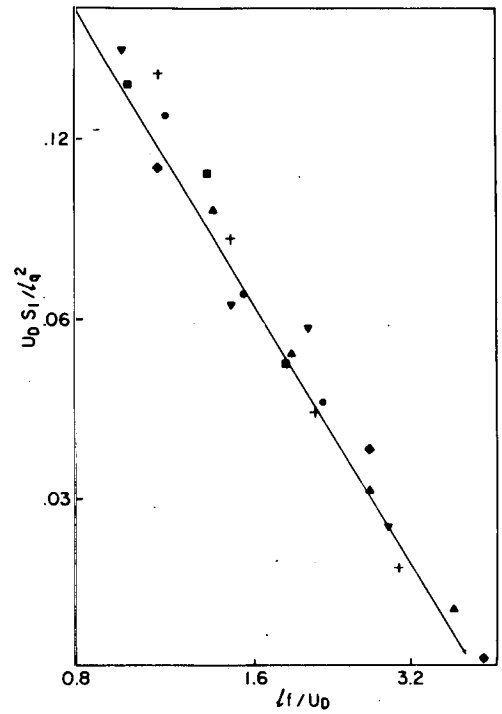

FIG. 7. Six low frequency spectra of the longitudinal turbulent velocity non-dimensionalized on the drift velocity U_D and dissipation length scale l versus non-dimensionalized frequency. The closed symbols denote (symbol, run, depth): (◆, 2, 82), (■, 3, 44), (▼, 3, 62), (+, 3, 69), (●, 4, 67), (▲, 4, 117). A line with slope $-5/3$ has been drawn for reference.

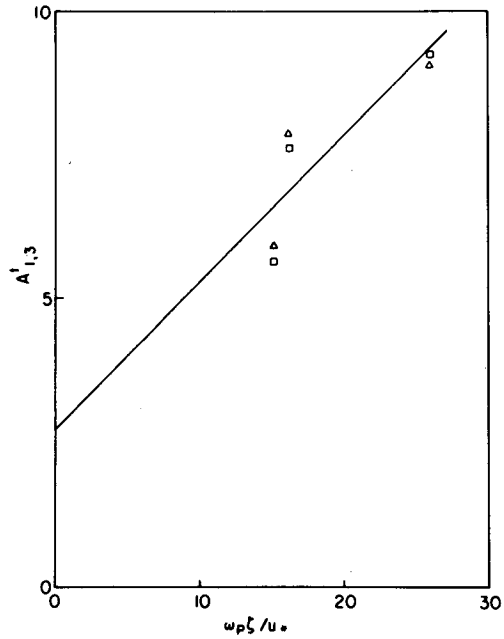

FIG. 6. Dependence of the magnitude of the longitudinal (A'_1) and vertical (A'_3) rms turbulent velocities, extrapolated to the surface ($z = 0$), on wave conditions using the exponential parameterization discussed in Section 7.

net dissipation in the layer is still less than the net energy input from the wind:

$$\int \epsilon dz < \tau_a c_{ph} \approx 650\ \text{cm}^2\ \text{s}^{-3}\ \text{[runs 3 and 4]}, \qquad (38)$$

where τ_a is the wind stress (see Eq. 19) and c_{ph} is the phase speed of waves in the peak of the narrow wave spectrum. Another concern is that the large values of ϵ might be a consequence of our use of linear filtration. However, ϵ has been determined from the low frequency behavior of the turbulent spectra. In this fre-

TABLE 5. Dissipation rates and length scales as determined from the low frequency portion of the longitudinal turbulent velocity spectra.

$$q^2 = \langle u_1'^2 + u_3'^2 \rangle/2, \quad Q^2 = \langle u_1^{w2} + u_3^{w2} \rangle/2$$

Run	z (cm)	U_D (cm s^{-1})	q (cm s^{-1})	Q (cm s^{-1})	ζ_{rms} (cm)	ϵ (cm^2 s^{-3})	l (cm)
2	82	2.9	9.0	20.0	15.7	4.8	150
	44	11.0	6.8	13.5	6.8	3.7	83
3	62	10.5	5.7	9.8	6.6	1.7	110
	89	12.5	4.1	6.2	6.5	0.7	101
	67	9.0	5.3	8.1	6.2	2.3	66
4	117	8.0	4.3	5.6	6.6	1.2	66

quency range the wave velocity spectra are an order of magnitude smaller than the turbulent intensities. We expect, therefore, that our values of ϵ are not very sensitive to the filtration procedure.

It is interesting to compare our estimates of the dissipation rate with those of Dillon (1981). The latter were obtained from high frequency temperature measurements under comparable wind–wave conditions, and are for the region $1.5 \leqslant z \leqslant 6$ m. Both the magnitude and depth dependence of the dissipation in this region are not inconsistent with a constant-stress layer [Eq. (37)]. Our measurements in the upper 1 m (just above Dillon's layer) show a much higher dissipation, suggesting that in this layer there are sources of turbulence in addition to shear. We consider (in the presence of stable stratification) that this source of turbulent energy can come only from the wave motion—either through breaking or wave–turbulence interaction, such as we have proposed in P1. The picture that emerges from these considerations is one of a two layer structure; the upper layer, with thickness of order $10\zeta_{\text{rms}}$, is a region of intense turbulence generation by waves, while below this region the more classical notion of a constant-stress layer is appropriate. Further indication of a two layer structure can be seen in the plots of rms turbulent intensity (Fig. 4), in which noticeable flattening is observed below 1.5 m. Finally, we note that if the turbulent layer of wave influence does not scale with the rms wave height, then in the presence of energetic wind waves in the open ocean this layer can extend some tens of meters.

The question then arises, at what scales and due to what mechanisms is the surface wave energy transformed to turbulent energy beneath wind waves. According to the variability of ϵ determined at frequencies lower than f_p the additional source of energy is at frequencies lower than wave peak frequency. The theory suggested in P1 shows that the energy flux to turbulence additional to the mean shear production can be determined by measuring the divergence of the third mixed moments of the fluctuating velocity field, or more exactly the divergence of the vertical wave energy flux due to turbulence, $\langle \sigma_w^2 u_3' \rangle$. It was also speculated in P1 that the main contribution to such third moments must come from frequencies *comparable* (or even lower) than the peak wave frequency. Therefore an attempt was made to estimate the values of $\langle (\sigma_w^2 u_3' \rangle$ and their vertical distribution from this data. However, a preliminary analysis of the drag sphere measurements indicated we did not obtain reliable data for the third moments of the fluctuating velocity field. According to the theory in P1, part of the contribution to $\langle \sigma_w^2 u_3' \rangle$ can be due to the correlation between ζ^2 and u_3'. Estimates of the values $\langle \zeta^2 u_3' \rangle$ have shown that in most of the cases the direction of wave energy flux is downwards, which is consistent with the theory. Estimates of the divergence of this flux were too unreliable to make with the present data. In order to obtain reliable values of $\langle \sigma_w^2 u_3' \rangle$, or even $\langle \zeta^2 u_3' \rangle$, the observations must cover a large enough range of frequencies both above and below the wave peak frequency. This will require more elaborate experiments in the future. That is why we decided to limit ourselves here to an analysis aimed only at demonstrating the presence of wave–turbulence interactions in the surface layer of the sea. However it is interesting to note that in run 3, which spans $0.44 < z < 0.89$ m, the depth dependence of ϵ is approximated very well by an exponential in z with a decay constant $\approx 3k_p$. Since the turbulence varies with depth on length scales comparable to that of the waves the decay of ϵ with z is consistent with the simple parameterization of the triple correlation presented in P1.

8. Comparison with the results of previous measurements of random velocity fluctuations beneath wind waves

We consider it instructive in this concluding section of the paper to discuss briefly the results of other measurements and their relation to our results.

There have been, of course, numerous attempts to make direct measurements of wave-induced (orbital) velocities in the ocean. Most of them, as for example the earliest measurements by Shonting (1964, 1968) and the more recent studies by Thornton and Krapohl (1974), Cavaleri, Ewing and Smith (1979), dealt only with a comparison of the observed velocity fluctuations with the predictions of the linear theory of surface gravity waves in the range of frequencies corresponding to the energy-containing components of the wind waves. The most interesting and controversial result of such measurements was an indication of the existence of a downward momentum flux, which was found in some cases to be even much greater (!) than the total atmospheric stress. According to the theory presented in P1, the conservation of the momentum in the upper ocean in the presence of waves implies (see Eqs. 15 and 16 of P1) that

$$\left.\begin{aligned} \partial_t \int_{-\infty}^{0} \rho U_\alpha dz = -\left(\rho\langle u_\alpha' w'\rangle - \mu \frac{dU_\alpha}{dz}\right)\Big|_{z=0} \\ -\left(\rho\langle u_\alpha' w\rangle - \mu \frac{dU_\alpha}{dz}\right)\Big|_{z=0} + \partial_t M_\alpha = \tau_{a\alpha} \end{aligned}\right\}, \quad (39)$$

where u_α' and w' are the horizontal and vertical components of the fluctuating velocity field, $M_\alpha = \langle u_\alpha'(0)\zeta\rangle$ can be considered as wave momentum [$u_\alpha'(0) \approx u_\alpha^w(0)$], and $\tau_{a\alpha}$ is the wind stress at the surface. It is clear that in statistically homogeneous situations [Eq. (39) was derived for this case] and during wind-wave generation conditions where $\partial M_a/\partial t > 0$, the measured correlation between u_α' and w' in the surface layer (not only at $z = 0$) cannot exceed the local surface stress $\tau_{a\alpha}$. Therefore some of the cited measurements are irrelevant for active wind–wave generation con-

ditions. Of course, when measured values of $\rho\langle u'_\alpha w'\rangle$ were comparable with the surface stress $\tau_{a\alpha}$, the authors attributed this to the effect of turbulence, without however separating the wave and turbulent components in the range of scales (frequencies) corresponding to the energy containing motions. So the question of which spectral components of the fluctuating motions were responsible for the downward momentum flux was not properly resolved in these studies.

Serious attempts to describe the turbulent motions in the presence of waves were made by Yefimov and Khristoforov (1969, 1971a,b). These authors used a specially devised orbital velocity sensor for the measurement of velocity fluctuations. However, even with improved frequency response, their velocimeter did not permit them to estimate the spectral components of the velocity fluctuations beyond a frequency of 1.0 Hz. The simultaneous measurements of the surface displacement $\zeta(t)$ and velocity fluctuations $\mathbf{u}'(z, t)$ showed that the coherence $\gamma^2_{i\zeta}(\omega)$ between them drops relatively rapidly past a transitional frequency $\omega = \omega_t$, which they chose as $\gamma^2_{i\zeta}(\omega_t) \approx 0.25$. Therefore Yefimov and Khristoforov simply considered the high-frequency ($\omega > \omega_t$) parts of the observed velocity spectra as due to small-scale, three-dimensional turbulence. They found the interesting result that the absolute values of the spectral densities of velocity fluctuations for $\omega \leq \omega_t$ were not noticeably attenuated with increasing depth, whereas the intensity of turbulence (e.g., spectral components with $\omega > \omega_t$) was always much smaller than the wave-induced motions ($\omega < \omega_t$). So the attenuation with depth of the intensity of this "small scale turbulence" was markedly different than for the wave motions. They also found that the energy level of the "high frequency small-scale turbulence" increased with increasing wave energy. Yefimov and Khristoforov attributed this to the dynamic interaction between turbulence and orbital shear (Kitaigorodskii 1961a,b). In some cases they even saw a peak in the frequency spectra of the velocity fluctuations at 1 Hz, but it was too small to be reliable. As was pointed out in P1 the extraction of wave energy in this manner is probably insignificant for the overall turbulent energy budget. The fortunate circumstance in Yefimov and Khristoforov's experiment was that the range of scales and depths covered in their study permitted them, without separating the velocity field into turbulent and wave-induced parts, to attribute the disappearance of coherence at high frequencies to the natural filtration of the orbital components by $\exp(-\omega^2 z/g)$. This was their justification for using the spectral correlation $\gamma^2_{i\zeta}$ as a tool to isolate those components ($\omega > \omega_t$) that are not related to surface waves and to identify them as "high-frequency" turbulence. In addition to the fact that this is a very subjective method, since it depends on the choice of the cutoff ω_t, their measurements also cover an insufficient range of frequencies ($0.5 < f < 1$ Hz) from which to determine a possible dynamical source of the surface layer turbulence. For example shear produced turbulence, usually with frequencies smaller than the peak wave frequency f_p, was not measured at all and the accuracy of their measurements did not allow them to see the modulation of the background turbulence by waves.

Measurements of the low-frequency part of the spectrum of velocity fluctuations ($f < 10^{-1}$ Hz) in the upper mixed layer were recently analyzed by Jones and Kenney (1977). They concluded that such data can be scaled reasonably well with the similarity variables for the constant flux layer, i.e. on friction velocity u_* and depth z. They interpreted this to indicate the presence of shear-generated turbulence occupying a frequency band between inertial oscillations and surface wave-induced motions. But they did not discuss the possibility of an additional energy input to the turbulence, even though their observed spectra have a noticeably different form at frequencies $f < 10^{-2}$ Hz.

We can thus summarize this discussion by stating that the spectra presented in this paper are the first reliable information about upper-layer turbulence in the presence of waves, and their shape can be explained to first order as "frozen" inertial range turbulence modulated by surface waves. Moreover the results of this study clearly show that the turbulent energy in the frequency band 10^{-2} Hz $< f < 10$ Hz, as well as the turbulent energy dissipation, cannot be explained solely within the framework of similarity theory for the inner (constant flux) layer and that the transformation of wave energy into turbulence must also be considered. It is for future experimental studies to shed light on the questions of how, and in what range of scales, this mechanism works.

Acknowledgments. We are grateful to several members of the technical and data processing staffs at the Canada Centre for Inland Waters for their assistance during the field trials and subsequent data analysis. In addition, D. C. Beesley operated the data recording system and we thank him for his continued assistance throughout the project.

Supported in part by the U.S. National Science Foundation under Grants ATM 79-22006 and CME 79-19817, in part by the U.S. Office of Naval Research under the following programs: Fluid Dynamics (Code 438), Power (Code 473) and Physical Oceanography (Code 481), and in part by the U.S. NASA–Ames Research Center under Grant MSG-2382.

REFERENCES

Benilov, A. Ju., 1978: The error of the linear filtration method in the analysis of the fluctuations of random fields of the near water atmospheric layer and the upper ocean. *Oceanology*, **18**, 28–34.

——, and B. W. Filyushkin, 1970: An application of the linear filtration technique for the analysis of fluctuations in the sea

surface layer. *Izv. Akad. Nauk SSSR, Ser. Fiz. Atmos. Okeana,* **6,** 810–819.

Birch, K. N., E. J. Harrison and S. Beal, 1976: A computer-based system for data acquisition and control of scientific experiments on remote platforms. *Proc. Oceans '76 Conf.,* Washington DC, 258–267.

Cavaleri, L., J. A. Ewing and N. D. Smith, 1978: Measurement of the pressure and velocity field below surface waves. *Turbulent Fluxes Through the Sea Surface, Wave Dynamics, and Prediction,* A. Favre and K. Hasselman, Eds., Plenum Press, 257–270.

Dillon, T. M., J. G. Richman, C. G. Hansen and M. D. Pearson, 1981: Near-surface turbulence measurements in a lake. *Nature,* **290,** 390–392.

Donelan, M. A., 1978: Whitecaps and momentum transfer. *Turbulent Fluxes Through the Sea Surface, Wave Dynamics and Prediction,* A. Favre and K. Hasselman, Eds., Plenum Press, 273–287.

——, 1982: The dependence of the aerodynamic drag coefficient on wave parameters. *First Int. Conf. on Meteorology and Air-Sea Interaction of the Coastal Zone.* The Hague, Amer. Meteor. Soc., 381–387.

——, and J. Motycka, 1978: A miniature drag sphere velocity probe. *Rev. Sci. Instrum.,* **49,** 298–304.

Jones, I. S. F., and B. C. Kenney, 1977: The scaling of velocity fluctuations in the surface mixed layer. *J. Geophys. Res.,* **82,** 1392–1396.

Kitaigorodskii, S. A., 1961a: Theory of turbulent mixing in the sea in connection with computing the depth of the upper isothermal layer. *Tr. Inst. Okeanol. Acad. Nauk SSSR,* **52,** 3–86.

——, 1961b: Small scale turbulence in the surface layer of the sea involved in developed wind-caused wave action. *Tr. Inst. Oceanol. Acad. Nauk SSSR,* **52,** 87–96.

——, 1973: *The Physics of Air-Sea Interaction.* Israel program for Scientific Translations Jerusalem (English translation). 237 pp. [NTIS TT-72-50062].

——, and J. L. Lumley, 1983: Wave-turbulence in the upper ocean. Part I: The energy balance of the interacting fields of surface wind waves and wind-induced three-dimensional turbulence. *J. Phys. Oceanogr.,* **13,** 1977–1987.

Lumley, J. L., and E. A. Terray, 1983: Kinematics of turbulence convected by a random wave field. *J. Phys. Oceanogr.,* **13,** 2000–2007.

Monin, A. S., and A. M. Yaglom, 1971, 1975: *Statistical Fluid Mechanics,* Parts I and II. The MIT Press, 1260 pp.

Ozmidov, R. V., 1968: Horizontal turbulence and processes of horizontal turbulent transport in the ocean. *Izv. Akad. Nauk SSSR, Ser. Fiz. Atmos. Okeana,* **4,** 1224–1225.

Shonting, D. H., 1965: A preliminary investigation of momentum flux in ocean waves. *Pure Appl. Geophys.,* **57,** 149–152.

——, 1968: Autospectra of observed particle motions in wind waves. *J. Mar. Res.,* **26,** 43–65.

Thornton, E. B., and R. F. Krapohl, 1974: Water particle velocity measured under ocean waves. *J. Geophys. Res.,* **79,** 847–852.

Yefimov, V. V., and G. N. Khristoforov, 1969: Some properties of the velocity field in the layer of wind-induced undulation. *Izv. Akad. Nauk SSSR Ser. Fiz. Atmos. Okeana,* **5,** 1036–1048.

——, ——, 1971a: Wave related and turbulent components of velocity spectrum in the top sea layer. *Izv. Akad. Nauk SSSR Ser. Fiz. Atmos. Okeana,* **7,** 200–211.

——, and ——, 1971b: Spectra and statistical relations between the velocity fluctuations in the upper layer of the sea and surface waves. *Izv. Acad. Nauk SSSR Ser. Fiz. Atmos. Okeana,* **7,** 1290–1310.